HOSTED BY

ELSEVIER

Contents lists available at ScienceDirect

Asian Pacific Journal of Tropical Disease

journal homepage: www.elsevier.com/locate/apjtd

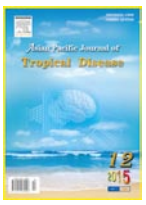

Original article doi: 10.1016/S2222-1808(15)60968-9

Physical, chemical and biological studies of gelatin/chitosan based transdermal films with embedded silver nanoparticles

Sneha Paul[1], Aiswarya Jayan[2], Changam Sheela Sasikumar[1*]

[1]*Department of Cellular and Molecular Biochemistry, Frontier Lifeline and Dr. K.M. Cherian Heart Foundation (Affiliated to University of Madras), R-30-C, Ambattur Industrial Estate Road, Mogappair, Chennai, Tamilnadu, 600101, India*

[2]*Department of Biotechnology, Karunya University, Coimbatore, Tamilnadu, 641114, India*

ARTICLE INFO

Article history:
Received 16 Oct 2015
Received in revised form 3 Nov 2015
Accepted 7 Nov 2015
Available online 13 Nov 2015

Keywords:
Chitosan-gelatin transdermal film
In vitro drug release
Dialysis membrane
Wound management
Anti-microbial
MTT
Reactive oxygen species generation
2'7'-Dichlorofluorescein diacetate

ABSTRACT

Objective: To study the physical, chemical and biological properties of composite chitosan-gelatin transdermal film along with silver nanoparticles as binding agent and determine the compatibility of the prepared amalgamation towards wound management.

Methods: Transdermal film preparations were done by solvent casting method containing different concentrations of biological synthesized silver nanoparticles. The films were characterized by using scanning electron microscope for their morphology and the determination of silver metal was done by using inductively coupled plasma atomic emission spectroscopy. Then a quantity of silver nanoparticles was further proceeded by physiochemical parameters (weight, thickness, temperature, solubility, absorption, tensile strength, *in vitro* drug release and skin permeation) and biological parameters studies (anti-microbial, cytotoxicity and reactive oxygen species).

Results: The film prepared by utilizing 2 g of gelatin and 0.5 g of chitosan exhibited better results. The physiochemical parameters studies revealed higher concentration of silver nanoparticles would give better results. *In vitro* drug release studies through dialysis and skin permeation showed the release of drug versus time (h). These films had shown excellent inhibition against *Streptococcus* and *Escherichia coli* species. Cytotoxicity study by MTT indicated the mild toxicity existed as the concentration of silver nanoparticles increased. Reactive oxygen species generation studies of transdermal film by using 2'7'-dichlorofluorescein diacetate assay demonstrated that the fluorescent cells were found in the higher concentration, which indicated cell damage (reactive oxygen species generated).

Conclusions: Based on these observations, *in vitro* performances against various characteristics of transdermal film, would be utilized as a distinct dressing material and patches accessible in market.

1. Introduction

Skin is an external barrier that provides us with a complete protection against bacterial infections, there by maintaining homeostasis of the body. Skin loss occurs frequently as a result of burns, trauma, and disorders as skin is the first organ coming in contact with the external factors. Commonly, wounds are distinguished into three categories such as superficial wound, partial thickness wound, and full thickness wound[1]. The basic principle of optimal wound healing is to minimize tissue damage, provide adequate tissue perfusion, oxygenation, proper nutrition, and moist wound healing environment to restore its biological function[2,3].

Traditionally, there are a lot of therapeutic options are available to treat wounds, but it takes prolonged time to heal. Due to recent advancements in the field of drug delivery, a rapid recovery can be observed against infections. The transdermal drug delivery is a new kind of drug delivery system that is being developed during recent times. Transdermal patch containing different constituents of drug substances pressed onto the skin is a non-invasive, convenient, and painless method for drug delivery and can also avoid major toxicities such as gastrointestinal toxicity[4,5].

Since 1960s, mushroom and its medicinal uses have been studied

*Corresponding author: Changam Sheela Sasikumar, Department of Cellular and Molecular Biochemistry, Frontier Lifeline and Dr. K.M. Cherian Heart Foundation, R-30-C, Ambattur Industrial Estate Road, Mogappair, Chennai, 600101, India.
Tel: +91-9283143681
E-mail: sheelsasic@yahoo.co.in

in detail for its medicinal value in traditional Chinese and Japanese medicine. The healing effects of mushrooms were recognized for thousands of years ago. For example, mushrooms like reishi, maitake, shitake, and Brazilian mushrooms have a long history of medicinal use[6]. Similarly, many medicinal mushrooms and their extracts have been widely studied for treating various disorders. *Ganoderma lucidum* (*G. lucidum*), a medicinal mushroom used in traditional Chinese medicine is known to have many beneficial effects and denoted as "healing mushroom". Especially its bioactive compounds possess strong anti-inflammatory properties[7-10].

Chitosan is the second most abundant natural biopolymer[11]. It has been used over a wide range of applications like wound healing agents, drug carriers, chelating agents, membrane filter for water treatment, and biodegradable coating or film for food packaging. It is also used as a potential biomaterial which can be used for nerve repair. Due to its film forming property, the chitosan solution can be easily fabricated to the nerve conduits and thereby promoting the repair of the peripheral nervous system[12].

Gelatin-based films are transparent, biodegradable and flexible. It is a suitable material to be blended with chitosan because of its ability to form hydrogen bonding with chitosan as it contains carboxyl groups on its backbone chain[11]. Silver nanoparticles are incorporated to enhance the antimicrobial properties and to increase the sterilization properties. In this study, we have developed the transdermal patch with chitosan-gelatin composite (C-GC) film embedded with silver nanoparticles to enhance the flexibility and to increase the strength of cross links, respectively.

2. Materials and methods

2.1. Chemicals, materials and samples

Gelatin and silver nitrate were purchased from Himedia Laboratories Pvt. Ltd. Glycerol, sodium hydroxide, hydrogen chloride, acetic acid, dithiothreitol, sodium dodecyl sulfate, ethylenediaminetetraacetic acid, glutaraldehyde and acetone were purchased from Fisher Scientific (Thermo Electron LLs India Pvt. Ltd.). Bacterial culture was purchased from American Type Culture Collection and the *Fenneropenaeus indicus* (Indian prawn) used in the experiment was collected from the local fish market, Chennai.

2.2. Isolation, extraction and purification of chitosan

The exoskeleton of the prawn shell was removed separately and rinsed thrice with tap water and twice with distilled water, respectively. They were then dried in the hot air oven for about 24 h at 55 ℃. The sample obtained was soaked in 4% boiling sodium hydroxide by using a 1 000 mL beaker for 1 h. The sample was then allowed to cool at room temperature for 30 min. After that, they were crushed further to small pieces of length 0.5–5.0 mm[13]. The obtained sample was demineralized by using 1% hydrochloric acid with 4 times its quantity and then soaked for 24 h to remove minerals. The above samples were treated with 50 mL of 2% sodium hydroxide for 1 h and the remains of them were washed with deionized water and then drained off[14]. The process was repeated by adding 50% sodium hydroxide to the obtained sample and boiling it for 2 h at 100 ℃. The sample was allowed to cool at room temperature for 30 min, and subsequently washed continuously with 50% sodium hydroxide. The obtained sample was filtered and filtrate was oven dried for 6 h at 110 ℃ to obtain the crude chitosan[15]. After that the obtained chitosan was purified to make it suitable for use. The purification process was designed in three steps; removable of insoluble with filtration, reprecipitation of chitosan with 1N sodium hydroxide and demetallization of retrieved chitosan[16].

2.3. Biosynthesis of silver nanoparticles

2.3.1. Preparation of G. lucidum extract

G. lucidum mushroom was collected (Indian Institute of Technology, Chennai), washed and dried till it was hard. The mushroom was shredded and mixed with double distilled water in the proportion of 20 g in 100 mL. Then the obtainded solution was conducted to boil for 2 min and subsequently filtered and stored at 4 ℃ until further use[17].

2.3.2. Preparation of the silver nanoparticles

A total of 35 mg of silver nitrate was added to 250 mL of water and the solution was uniformly mixed. To obtain silver colloids, 10 mL of the mushroom extract and 90 mL of the silver nitrate solution were mixed and incubated for 1 h at room temperature. The confirmation of silver nanoparticles was confirmed by the appearance of light yellow colour to dark brown on complete reduction. The pH of the solution was adjusted to around 7.5. Sample was read under UV-visible spectrometer for the presence of silver nanoparticles[18,19]. The confirmation of silver nanoparticles was done by using various analytical techniques such as transmission electron microscopy (TEM), energy dispersive X-ray analysis (EDAX), and X-ray diffraction (XRD).

2.4. Preparation of C-GC transdermal film

A series of C-GC transdermal films was prepared by varying the ratio of constituents[20]. The values obtained were then optimized (Table 1).

Table 1
Value optimization of C-GC transdermal film.

Composition	Varied concentrations						
	C1	C2	C3	C4	C5	C6	C7
Chitosan (g)	0.5	1.0	1.5	2.0	2.5	3.0	3.5
Glycerol (μL)	100	200	400	800	1 000	1 200	1400
Gelatin (g)	0.5	1.0	1.5	2.0	2.5	3.0	3.5
Silver NPs (μL)	100	200	400	800	1 600	3 200	6 400
Water (mL)	10	15	20	25	30	35	40

NPs: Nanoparticles; C1–C7: A series of C-GC films with different concentrations.

2.5. Characterizations

Fixation of the C-GC transdermal film was done with 4% glutaraldehyde for 2 h. Then it was implemented by serial washes and finally kept for drying. The surface morphology of the C-GC transdermal film was analyzed by using scanning electron microscope (SEM) and determination of silver metal by using inductively coupled plasma atomic emission spectroscopy (ICP-OES).

2.6. Physiochemical properties of C-GC transdermal film

2.6.1. Size and thickness/weight

The film thickness was measured by using a digital vernier screw gauge (Ultra Science Aids, Bangalore, India) at various areas of the films and the average thickness was calculated[21].

2.6.2. Water solubility

The water solubility of each film was determined by immersing a small piece of the film in distilled water for 24 h. The samples were cut randomly from each film and placed in different test tubes containing 1 mL of distilled water. Readings were noted at every consecutive hours[21].

2.6.3. Water absorptivity and humidity

Six different films each of 1 cm were weighed (initial weight) separately and equilibrated with distilled water for 1 week. Three films were exposed to ambient conditions of humidity and the other three were exposed to saturation humidity conditions at room temperature for 2 days. Then weight of each film (final weight) was determined to calculate the gained weight of each film[21]. Percent moisture absorption was calculated by using the following equation:

$$\text{Percent moisture absorption} = \frac{(\text{Final weight - initial weight}) \times 100}{\text{Initial weight}}$$

2.6.4. Temperature and pH

The capacity of the C-GC transdermal film to withstand the temperature was determined by placing the film in a hot water bath with varying temperature (10–100 ℃) and pH was also recorded for withstand capability.

2.6.5. Tensile strength

The tensile strength and elongation of each film–type sample were determined with an Instron universal testing machine (Model 5565, Instron Engineering Corporation, Canton, USA). Rectangular specimens (2.54–15.00 cm) were cut by using a precision double-blade cutter (Model LB.02/A, Metrotec, S.A., San Sebastian, Spain). Initial grip separation was set at 50 mm/min, and cross-head speed was set at 50 mm/min. The tensile strength and elongation measurements for each type of film were taken as follows: one sheet of each type of film was used with two to three specimens cut from each sheet of film and then the graph was recorded[21].

2.6.6. Folding endurance

The folding endurance of the C-GC transdermal film was evaluated individually by folding and opening the transdermal film repeatedly for 250 times at the same place or until a break developed in the place of folding.

2.6.7. In vitro drug release

The *in vitro* drug release method was done to determine the percentage/concentration of the drug released from the transdermal film through the skin and here little modification was made[22-24].

2.6.8. In vitro skin permeability

The skin permeability study was done here with chicken skin. The fat and hair of the chicken skin was removed by soaking it into 0.32 mol/L of ammonia solution for about 1 h. The skin was then kept in contact with the phosphate buffer saline (PBS) on a 1000 mL glass beaker. And on top of the skin, the transdermal film was kept. Then 1 mL of PBS solution was taken at the interval of every 4 h to study the permeability of the drug towards the skin. The measurement was taken at 376 nm by UV-vis spectrophotometer.

2.6.9. In vitro release of drug from the polymer

The *in vitro* release of drug from the biopolymer was investigated with the help of dialysis bag. The phosphate buffer was prepared and all components of the film were added in liquid form into the dialysis bag and then the dialysis bag was tied at both the ends where one was tied to the magnetic stirrer and the other end was left free so that it could be also rotate along with the stirrer. Then 1 mL of phosphate buffer solution was taken at the interval of every 4 h to study the release of the drug from the polymer. The measurement was taken at 376 nm by UV-vis spectrophotometer.

2.7. Biological properties of C-GC transdermal film

2.7.1. Antibacterial studies by well diffusion and disc diffusion assays

The antibacterial assays were done on human pathogenic bacteria. The nutrient agar medium was poured into Petri plates. After allowing the medium to solidify, 1 mL of bacterial inoculum was placed on the plates and spread with cotton swabs. In well diffusion method, 6 wells around 10 mm diameter were cut out aseptically with the help of a cork borer. Each well was filled with different concentrations of C-GC transdermal film. In disc diffusion method, different concentrations of C-GC transdermal film were placed on the plates. Plates were incubated at 37 ℃ for 24 h and zone of inhibition was noted[19].

2.7.2. Cell line maintenance

The Vero cell line was obtained from King's Institute, Chennai, and 3T3-L1 fibroblast cell line was obtained from National Center for Cell Sciences, Pune. The cell line was maintained in Dulbecco's modified Eagle medium supplemented with 10% fetal bovine serum,

100 μg/mL penicillin and 100 μg/mL streptomycin and then placed in CO_2 incubator.

2.7.3. MTT assay

The MTT dye reduction assay was performed to determine the cytotoxic effect of the C-GC transdermal films. The assay depended on the reduction of MTT by mitochondrial dehydrogenase, an enzyme present in the mitochondria of viable cells, to a blue formazan product. The cell concentration was adjusted to 1×10^5 cells/mL and plated onto 96-well flat bottom culture plates with different concentration of C-GC transdermal film. All cultures were incubated for 24 h at 37 ℃ in a humidified incubator. After 24 h of incubation (37 ℃, 5% CO_2 in a humid atmosphere), 10 mL of MTT (5 mg/mL in PBS) was added to each well and the plate was incubated for a further 4 h at 37 ℃. The resulting formazan was dissolved in 100 mL of dissolving buffer (provided as part of the kit) and absorbance of the solution was read at 595 nm by using an ELISA reader. All determinations were carried out in triplicate. Concentrations of transdermal films showing 50% reduction in cell viability (*i.e.*, IC_{50} values) was then calculated[25].

2.7.4. 2'7'-dichlorofluorescein diacetate (DCF-DA) dye preparation

A total of 5 mmol/L of DCF-DA was diluted in 5 mL of dimethylsulfoxide, then mixed with 0.1 mmol/L of Evans blue dye. It was stored at -20 ℃ under dark condition.

2.7.5. Reactive oxygen species (ROS) generation assay

The most common probe used for the detection of intracellular ROS formation is DCF-DA. DCF-DA was cell permeable, trapped with the cells and converted to 2′,7′-dichlorofluorescein (DCF), a fluorescent molecule. The fibroblast cell line was taken with 60%–70% confluence for the studies and each well was substituted by different concentrations of C-GC transdermal film. One well left as control and another well processed as negative control that induced by H_2O_2 incubated for 6 h at CO_2 cell incubator. After incubation, 2 mL of DCF-DA dye was added and kept for 30 min at 37 ℃, the sample was then rinsed by PBS and air dried and viewed under a fluorescence microscope (blue filter, 485–590 nm, WL)[26].

2.8. Statistical analysis

Data pertaining to physiochemical properties and applications of transdermal films were expressed as mean ± SEM, $n = 6$ and the data were analyzed by One-way ANOVA using GraphPad Prism version 6.00 for Windows (GraphPad Software, La Jolla California, USA). In all the analysis, $P < 0.05$ was considered as statistically significant.

3. Results

3.1. Synthesis and characterization of silver nanoparticles

Approximately after 30 min of incubation along with *G. lucidum* the silver nitrate started to reduce into silver nanoparticles that demonstrated by change of colour from yellow to intense brown colour (Figure 1). At that point the change of colour in the samples was read by double beam spectrophotometer from 300–700 nm, the most prominent peak was observed at 418 nm (Figure 2).

Figure 1. The reduction of silver nitrate to silver nanoparticles by addition of mushroom extract.

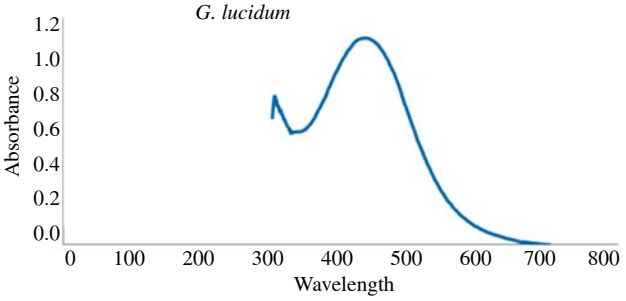

Figure 2. UV-vis absorbance spectra of silver nitrate solution with aqueous extracts of sample after their reduction.

Photographs from TEM, confirmed the spherical shape of silver nanoparticles synthesized by *G. lucidum* (Figure 3A). The silver nature of crystalline nanoparticles was confirmed by selected area electron diffraction (SAED) pattern (Figure 3B) and at higher magnification, the nanoparticles were clearly recognized and the size of each nanoparticle crystal domain was around 10–50 nm.

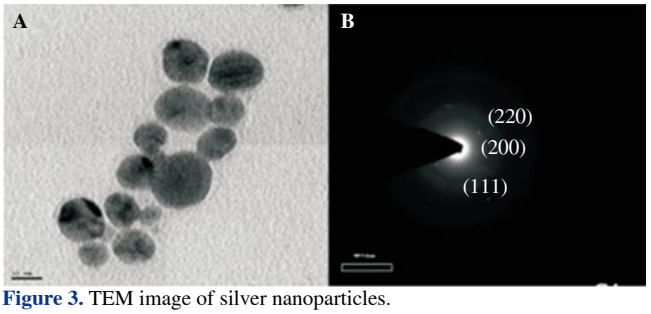

Figure 3. TEM image of silver nanoparticles.
A: The spherical shape of silver nanoparticles; B: The silver nature of crystalline nanoparticles confirmed by SAED pattern.

The EDAX of silver nanoparticles confirmed the elemental composition of nanoparticles as silver (Table 2 and Figure 4). The biosynthesized silver nanoparticles were further subjected to XRD. The XRD pattern showed three distinct peaks at respective 2θ value known for zero-valent face centered cubic silver representing the (111), (200), (210) crystal planes due to that Bragg's reflections were present and hence confirmed the shape of the sample (face centered cubic). The average size of nanoparticles was calculated by Scherer formula and found to be 75 nm size. In addition to the Bragg peaks, unassigned peaks were also observed suggesting that the crystallization of bio-organic phase occured on the surface of the silver nanoparticles (Figure 5). Fourier transform infrared spectroscopy (FTIR) spectroscopy was used to determine the functional groups present during the biosynthesis of silver nanoparticles (Figure 6). The spectrum revealed the band at 1 645.9 cm^{-1} that corresponded to amide I and II bands of amino acids and proteins, while corresponding bands were indicated at 2 929.3, 2 370.4, 2 065.5, 3 452.3, 3 750.1 cm^{-1}; symmetric and asymmetric CH_3 stretching and NH stretching, respectively. Then two bands were observed at 1 101.4 and 1 464.8 cm^{-1} assigned to CO stretching, CH_2 bending and CH_3.

Table 2

Components present in *G. lucidum*.

Element	Weight (%)	Atomic (%)
O K	1.37	2.37
Na K	0.15	0.19
Al K	89.45	91.71
K K	0.61	0.43
Ag L	6.11	1.57
Ac M	0.89	0.11
Totals	100.00	100.00

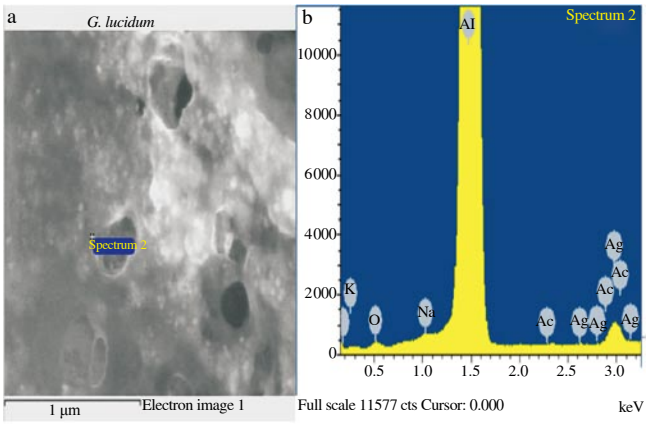

Figure 4. Image taken in EDAX (a) and the graph showed the components (b).

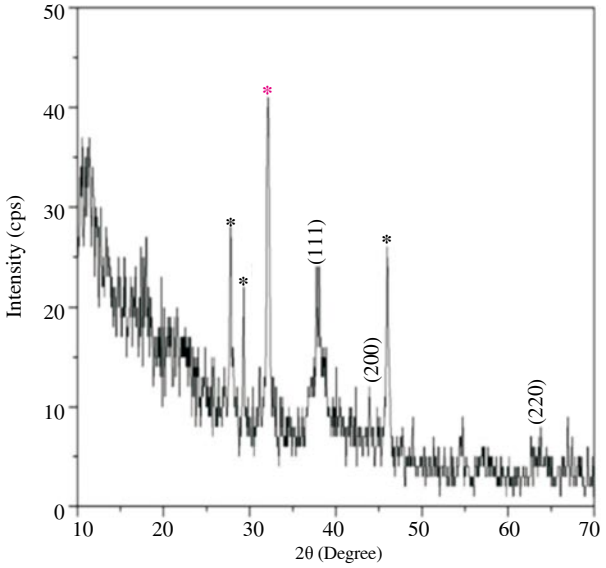

Figure 5. XRD spectrum of silver nanoparticles from *G. lucidum*.
*: Unassigned peaks.

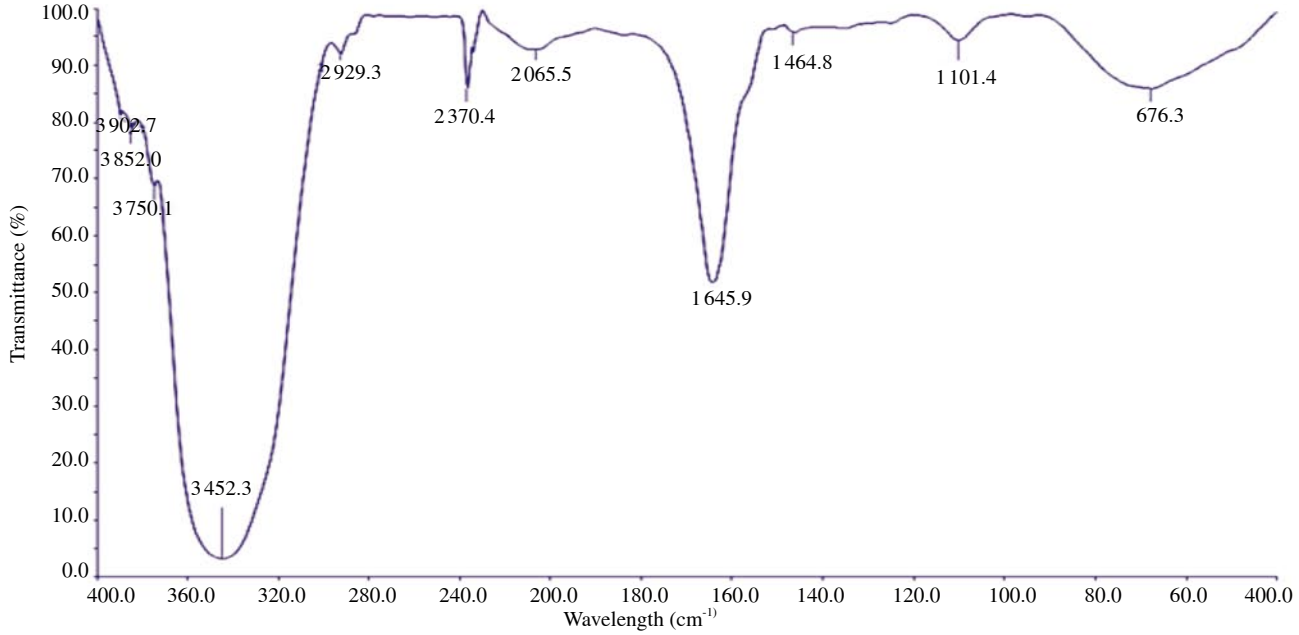

Figure 6. FTIR spectrum of silver nanoparticles + *G. lucidum*.

3.2. Analysis of physiochemical properties and characterization of chitosan

Chitosan was isolated from prawn shell as mentioned above, and the yield of chitosan from prawn shell was found to be 57.69% after purification. The results of physicochemical and functional properties of the prepared chitosan were moisture content 4%, ash value 1.86, loss on drying 2%, pH 6.7, solubility was by 2%-4% acetic acid.

The FTIR studies showed the major absorption band between 1 220 and 1 020 cm^{-1} which represented the free amino group (-NH_2) at C2 position of glucosamine, a major group present in chitosan. Further, the sample showed the absorption bands at the various peaks 712, 880.6, 1 026, 1 432, 1 576.2, 1 652.8, 2 927.0, 3 446.4 which were similar to standard chitosan. This confirmed the presence of chitosan (Table 3).

Table 3
Wavelength of main bands obtained from chitosan.

Vibration modes	Standard	Indian prawn
NH out-of-plane bending	752	712.0
Ring stretching	896	880.6
Co stretching	1 026	1 026.0
CH_2 bending and CH_3 deformation	1 418	1 432.0
Amide II band	1 563	1 576.2
Amide I band	1 661	1 652.8
Symmetric CH_3 stretching & Asymmetric CH_3 stretching	2 930	2 927.0
NH stretching	3 268	3 446.4

XRD studies were also done to confirm the formation of chitosan and to determine the nature of chitosan powder. XRD patterns of chitosan are illustrated in Figure 7 and exhibited broad diffraction peaks at 2θ = 10° and 21°.

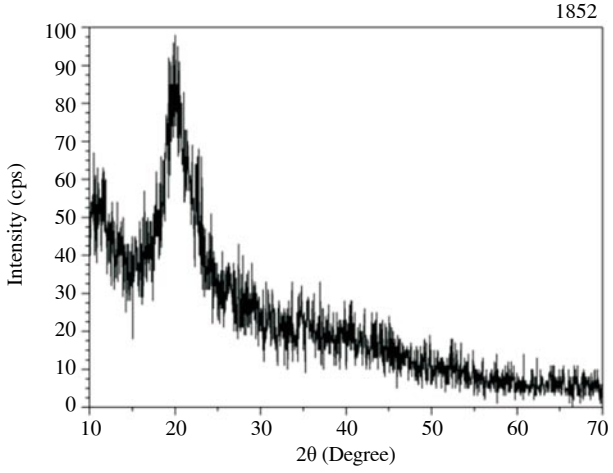

Figure 7. XRD pattern of chitosan.

3.3. Formation of C-GC transdermal film

All transdermal films prepared were colourless and transparent (Figure 8). The morphology of the chitosan-gelatin film was analyzed by SEM, the photograph showed a smooth surface with tiny particles that might be silver nanoparticles which had been coated (Figure 9). ICP-OES was used to determine the concentration of silver nanoparticles incorporated into C-GC film (Table 4).

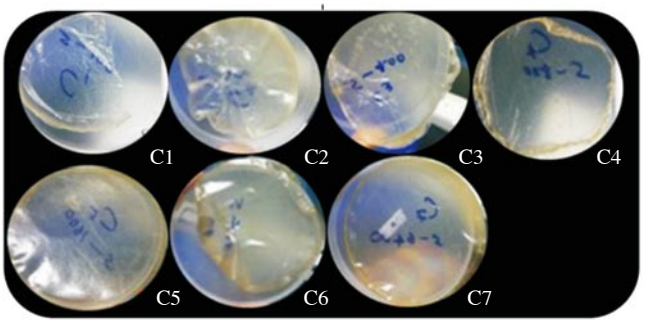

Figure 8. C-GC film incorporated with silver nanoparticles.

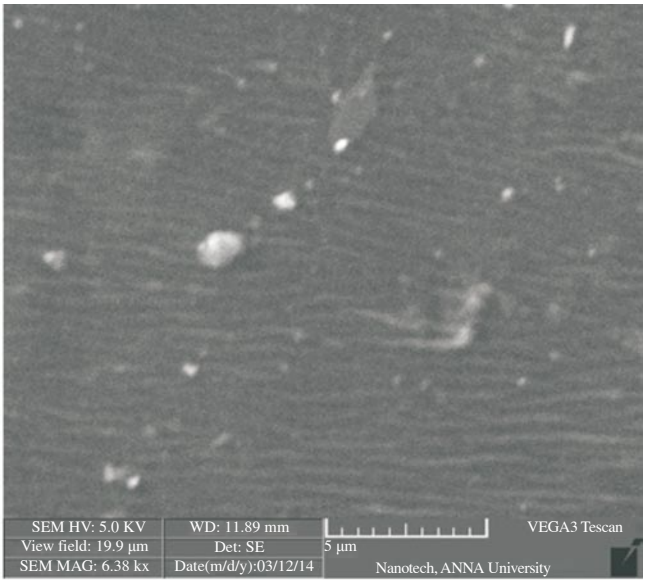

Figure 9. SEM image of the transdermal film.

Table 4
The concentration of silver nanoparticles by ICP-OES .

Samples	Elemental symbol	Concentration of silver nanoparticles (mg/L)
C1	328.068	0.245
C2	328.068	0.491
C3	328.068	0.986
C4	328.068	1.967
C5	328.068	3.935
C6	328.068	7.870
C7	328.068	15.740

3.4. Optimization studies

Optimization studies with varying concentration of compounds (chitosan, gelatin, glycerol, silver nanoparticles, distilled water) were studied to check the stability, elongation and stress holding capacity of chitosan-gelatin transdermal. The standard results showed in Table 5.

Table 5
Results of the various values optimized.

Composition	Varied concentrations						
	C1	C2	C3	C4	C5[+?]	C6	C7
Gelatin[*] (g)	2	2	2	2	2	2	2
Chitosan[*] (g)	0.5	0.5	0.5	0.5	0.5	0.5	0.5
Glycerol[*] (μL)	400	400	400	400	400	400	400
Distilled water[*] (mL)	30	30	30	30	30	30	30
Silver NPs (μL)	100	200	400	800	1 600	3 200	6 400

NPs: Nanoparticles; [*]: Standard value.

3.5. Physiochemical properties

The weight and thickness/size of the film were taken from different perimeters of the film to determine the uniformity of drug distribution in the film. In Figures 10 and 11, there is little non uniformity of drug in the film observed.

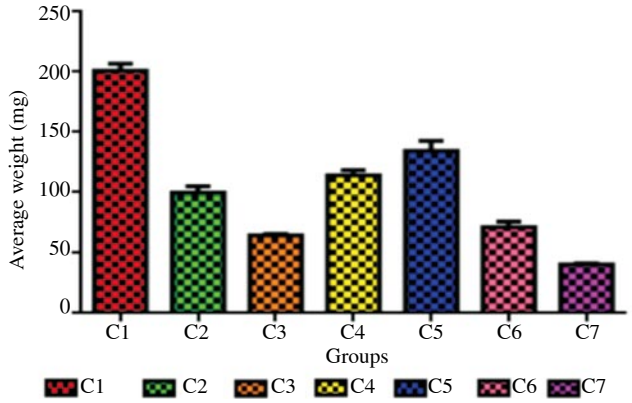

Figure 10. The average weight of film at different concentrations.

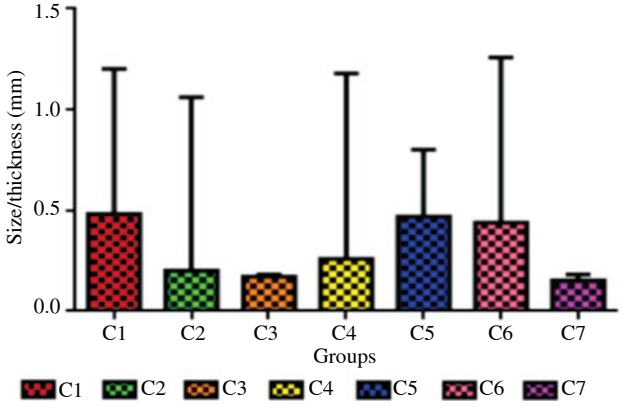

Figure 11. The average size/thickness of film at different concentrations.

Folding endurance parameter taken in account of determining the maximum stress managed by the film at the maximum number of times it was folded and at the point it broked. From Figure 12, we can observe that as the concentration of silver nanoparticles increasing, the stability of the film was significantly increased ($P < 0.05$).

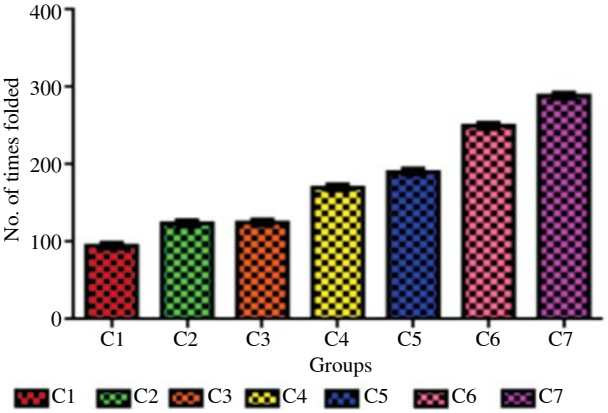

Figure 12. The folding endurance of film at different concentrations.

Humidity parameter study was done to determine the humidity absorption from the environment. The humidity of film increased significantly ($P < 0.05$) with the increasing of concentration (Figure 13). Temperature and pH were checked to determine the degree or pH at which the film was soluble/stable (Tables 6 and 7).

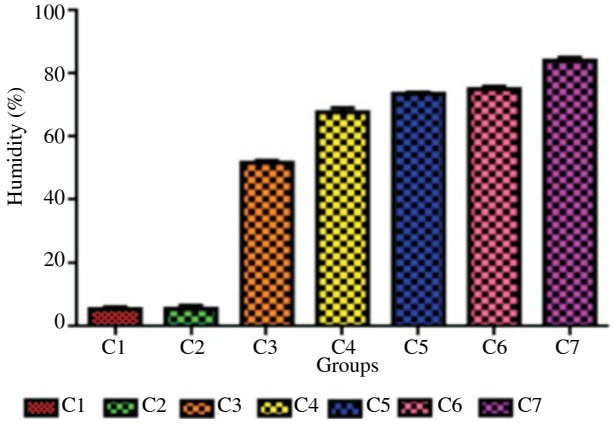

Figure 13. The humidity of film at different concentrations.

Table 6
The temperature of film at different concentrations.

Varied concentration	Varied temperatures (°C)								
	20	30	40	50	60	70	80	90	100
C1	NS	NS	NS	SS	SS	D	S	S	S
C2	NS	NS	NS	SS	SS	D	S	S	S
C3	NS	NS	NS	SS	SS	D	S	S	S
C4	NS	NS	NS	SS	SS	D	S	S	S
C5	NS	NS	NS	SS	SS	D	S	S	S
C6	NS	NS	NS	NS	NS	NS	D	D	D
C7	NS	NS	NS	NS	NS	NS	NS	D	D

NS: Not soluble; SS: Semi-soluble; D: Dispersed; S: Soluble.

Table 7
The pH of film at different concentrations.

Varied concentration	Varied pH values								
	1–2	2–3	3–4	4–5	5–6	6–7	7–8	8–9	9–10
C1	SS	SS	SS	SS	SS	S	L	L	L
C2	SS	SS	SS	SS	SS	S	L	L	L
C3	SS	SS	SS	SS	SS	S	L	L	L
C4	SS	SS	SS	SS	SS	S	L	L	L
C5	SS	SS	SS	SS	SS	S	L	L	L
C6	SS	SS	SS	SS	SS	S	L	L	L
C7	SS	SS	SS	SS	SS	S	L	L	L

SS: Semi-solid and film formed was delicated; S: Solid and proper film was formed; L: Film formed was hard/brittle.

The film's absorption of water and the solubility in the water were determined to check the distribution of drug to the site (Figures 14 and 15). The tensile study was done to show the strength, elongation and maximum tearing capacity of the film. The higher the concentration of the silver nanoparticle, the higher the elongation and flexibility of the sample would be, and silver also acted as strong cross linker in the formation of film (Figure 16).

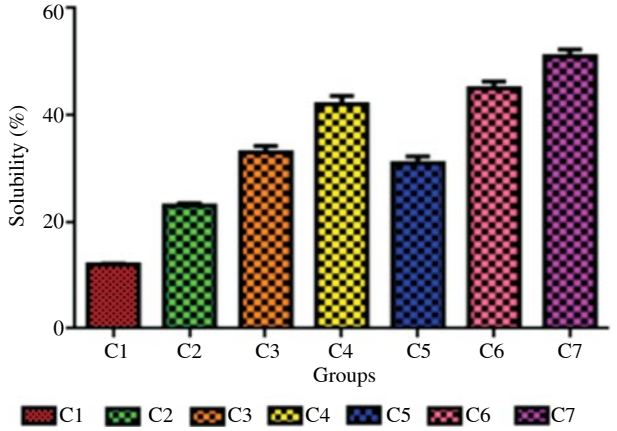

Figure 14. The solubility of the film at different concentrations.

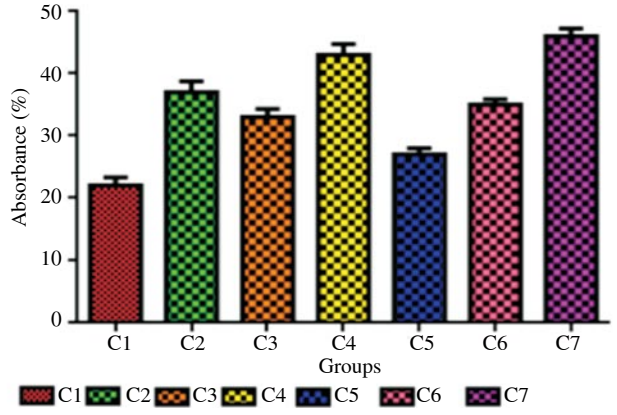

Figure 15. The absorbance of film at different concentrations.

3.6. *In vitro* release of drug from the polymer and in vitro skin permeability study

In vitro studies of drug released from the polymer and the skin permeation were done to determine the percentage of drug release through the dialysis membrane or skin and the time taken for the release was noted (Figures 17 and 18). The rate of release of silver nanoparticles obeying zero order kinetics and the release of drug from film were significantly increased ($P < 0.05$), expressed or released versus time (h).

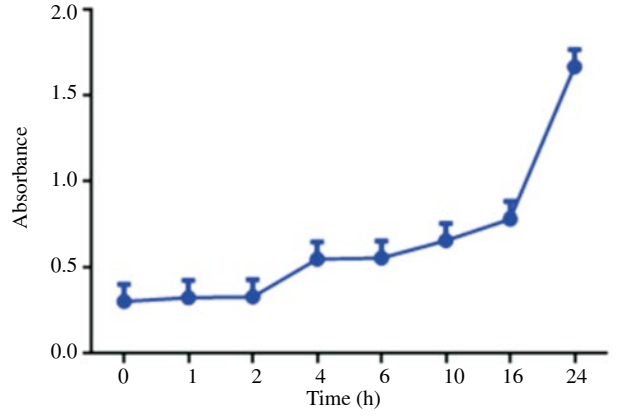

Figure 17. *In vitro* release of drug from the polymer film at different concentrations.

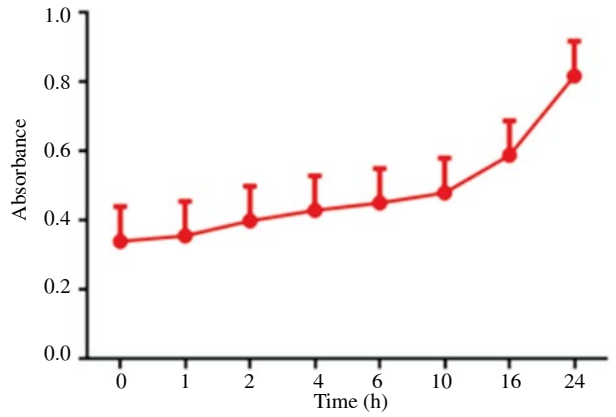

Figure 18. *In vitro* skin permeation of film at different concentrations.

3.7. Antimicrobial assay

The antimicrobial properties of chitosan-gelatin films incorporated with silver nanoparticles were presented in Figure 19 and Table 8. C-GC films showed an inhibition towards *Escherichia coli* (*E. coli*) and *Streptococcus* sp. of the tested microorganism. The more prominent zone was seen at the higher concentration of silver nanoparticles embedded in transdermal film.

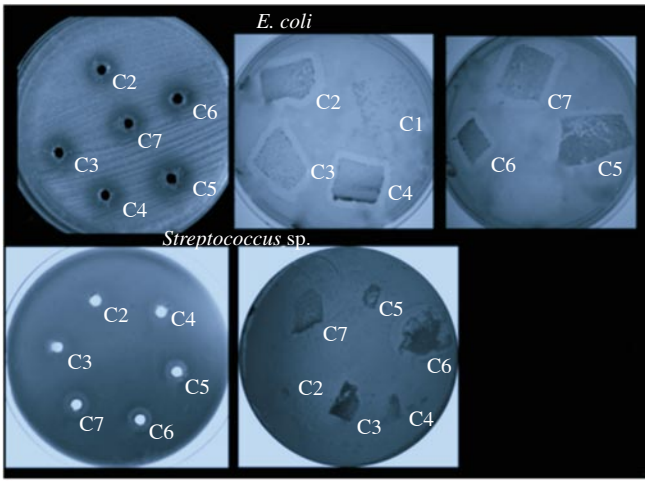

Figure 19. Viability of C-GC film incorporated with silver nanoparticles against various pathogenic microorganisms.

Table 8
Zone of inhibition of C-GC transdermal film. mm.

MTCC culture	C1	C2	C3	C4	C5	C6	C7
E. coli	-	8	10	11	14	14	14
Streptococcus sp.	-	< 8	< 8	8	8	10	12

3.8. *In vitro* cytotoxicity assay

The assay was used to evaluate the cytotoxicity effect of transdermal film against the Vero cell line. The different concentrations of C-GC transdermal film samples (C1–C7) were used. After 24 h incubation, cell viability was determined by MTT assay. The cytotoxicity was fully dependent on the concentration of gradient as the concentration increased mild toxicity was illustrated (Table 9).

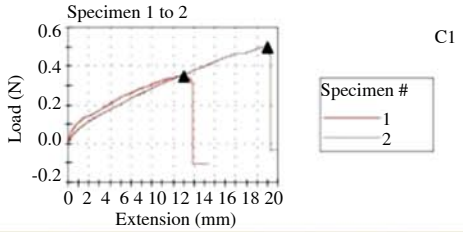

C1

	Diameter (mm)	Maximum load (N)	Tensile stress at maximum load (MPa)	Tensile extension at maximum load (mm)	Modulus (automatic young's) (MPa)
1		0.35	1.59	11.02	10.25
2		0.50	1.57	19.03	2.75
Maximum		0.50	1.59	19.03	10.25
Maximum		0.35	1.57	11.02	2.75
Mean		0.42	1.58	15.03	6.50
Standard deviation		0.11	0.02	5.67	5.31

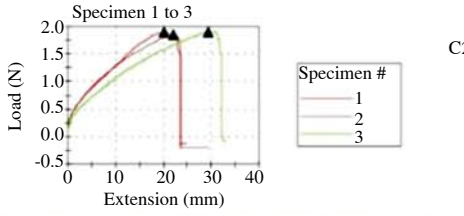

C2

	Diameter (mm)	Maximum load (N)	Tensile stress at maximum load (MPa)	Tensile extension at Maximum load (mm)	Modulus (automatic young's) (MPa)
1		1.89	2.31	20.10	10.01
2		1.84	2.77	22.20	12.45
3		1.89	2.97	29.33	8.13
Maximum		1.89	2.97	29.33	12.45
Maximum		1.84	2.31	20.10	8.13
Mean		1.88	2.68	23.88	10.20
Standard deviation		0.03	0.34	4.84	2.17

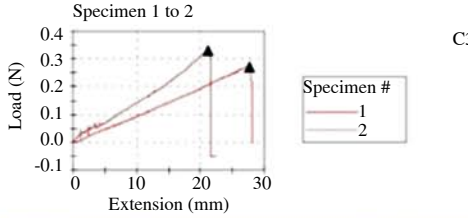

C3

	Diameter (mm)	Maximum load (N)	Tensile stress at maximum load (MPa)	Tensile extension at maximum load (mm)	Modulus (automatic young's) (MPa)
1		0.27	1.44	27.63	0.60
2		0.33	1.71	21.22	1.05
Maximum		0.33	1.71	27.63	1.05
Maximum		0.27	1.44	21.22	0.60
Mean		0.30	1.58	24.42	0.83
Standard deviation		0.04	0.19	4.54	0.32

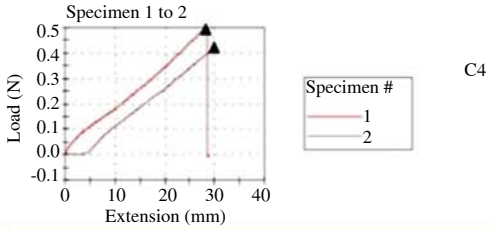

C4

	Diameter (mm)	Maximum load (N)	Tensile stress at maximum load (MPa)	Tensile extension at maximum load (mm)	Modulus (automatic young's) (MPa)
1		0.49	2.73	28.25	1.06
2		0.42	2.55	30.01	1.29
Maximum		0.49	2.73	30.01	1.29
Maximum		0.42	2.55	28.25	1.06
Mean		0.46	2.64	28.13	1.18
Standard deviation		0.05	0.13	1.24	0.16

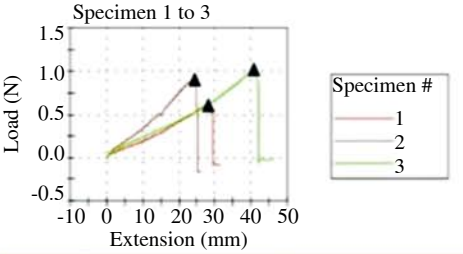

C5

	Diameter (mm)	Maximum load (N)	Tensile stress at maximum load (MPa)	Tensile extension at maximum load (mm)	Modulus (automatic young's) (MPa)
1		0.62	2.46	28.23	2.03
2		0.90	2.84	24.20	3.08
3		1.02	2.55	40.93	1.72
Maximum		1.02	2.84	40.93	3.08
Maximum		0.62	2.46	24.20	1.72
Mean		0.85	2.62	31.12	2.27
Standard deviation		0.21	0.20	8.73	0.71

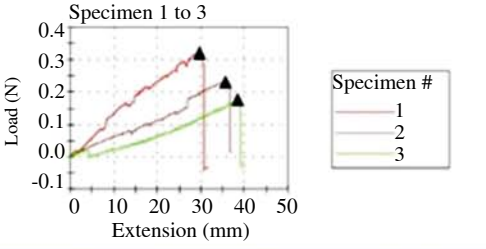

C6

	Diameter (mm)	Maximum load (N)	Tensile stress at maximum load (MPa)	Tensile extension at maximum load (mm)	Modulus (automatic young's) (MPa)
1		0.32	1.02	29.78	0.83
2		0.23	1.56	35.77	0.88
3		0.18	0.98	38.38	0.87
Maximum		0.32	1.56	38.38	0.88
Maximum		0.18	0.98	29.78	0.83
Mean		0.24	1.19	34.64	0.86
Standard deviation		0.07	0.32	4.41	0.02

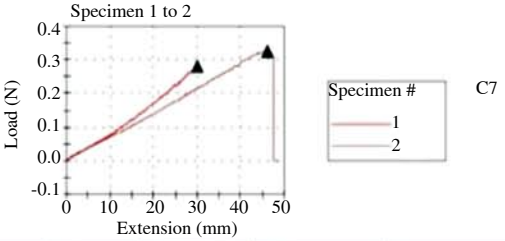

C7

	Diameter (mm)	Maximum load (N)	Tensile stress at maximum load (MPa)	Tensile extension at maximum load (mm)	Modulus (automatic young's) (MPa)
1		0.28	0.04	30.03	0.02
2		0.33	1.90	46.08	0.71
Maximum		0.33	1.90	46.08	0.71
Minimum		0.28	0.04	30.03	0.02
Mean		0.30	0.97	38.06	0.36
Standard deviation		0.03	1.31	11.35	0.48

Figure 16. Tensile study of C-GC film (C1–C7) incorporated with silver nanoparticles.

Table 9
In vitro cell toxicity study by using Vero cell line.

Concentration	Optical density value	Cell inhibition (%/mL)	Cell viability (%/mL)
C1	0.204	21.0	79.0
C2	0.169	39.0	61.0
C3	0.173	40.3	59.0
C4	0.142	49.9	50.0
C5	0.103	63.7	36.3
C6	0.700	75.3	24.7
C7	0.025	91.0	8.8
IC_{50} value	C4 (800 µL)		

3.9. DCF-DA assay

In this assay, the ROS generation was observed by substituting the different concentrations of transdermal film in the fibroblast cell line and the negative control was run by H_2O_2. Positive control was maintained with fresh media. In Figure 20, positive control cells didn't show any fluorescence, whereas negative control (induced by H_2O_2) cells showed almost 90%–99% ROS generation which means cell damage. The cells treated with samples C2, C4 and C6, respectively, C2 and C4 showed no signs of fluorescence cells, whereas in C6 fluorescence cells were observed at the range of 50%–60% and non-fluorescence were in the range of 40%–50%. Therefore, the higher concentration might prove toxic to the cells but average concentration showed no signs of toxicity. Hence, it could be taken for further studies.

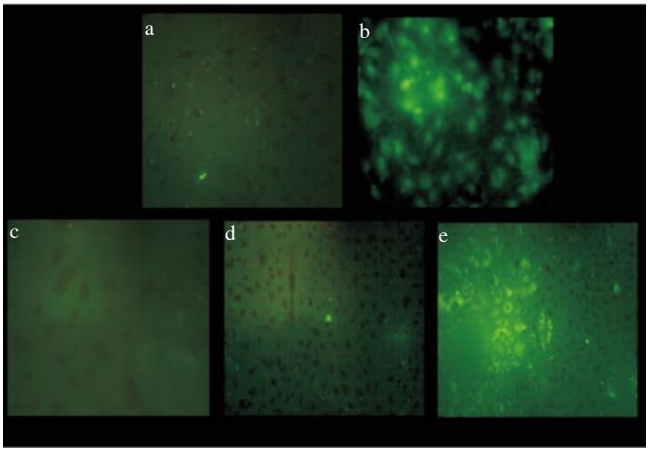

Figure 20. DCF-DA assay was done on 3T3-L1 (Fibroblast) cell line.
a: Positive control (cells + media); b: Negative control (cells + H_2O_2); c: C2 (cells + chitosan-gelatin transdermal film); d: C4 (cells + chitosan-gelatin transdermal film); e: C6 (cells + chitosan-gelatin transdermal film).

4. Discussion

There are several methods for synthesizing silver nanoparticles. In this study, biosynthesis of silver nanoparticles was carried out by using *G. lucidum* extract. The mushroom extract incubated with deionized water (positive control) retained its original colour (pale yellow) but silver nitrate treated with mushroom extract turned to brown colour after 30 min incubation due to deposition of silver nanoparticles. The colour development of the extract is due to excitation of surface plasmon resonance in the metal nanoparticles[27]. The colour of the solution was changed to intense brown after 24 h of incubation. The extract was also stable for maximum 2 months.

The progress of the reaction between metal ions and the extracts was examined by UV-vis spectra of silver nanoparticles in aqueous solution. The intensity of the colour increased with incubation time. Nanoparticles size can also be determined by the change in the colour of the reactant[28,29]. The smaller the size of nanoparticles greater the colour shifts towards reddish brown.

Transmission electron microscope photographs showed well documented size and shape of biosynthesized silver nanoparticles and also revealed the nature of silver crystalline by SAED pattern; signified by 3 different planes (111, 200, 220). The elemental composition of the nanoparticles was further confirmed by the EDAX. The peaks of silver around 3 keV observed in EDAX of the sample corresponded to the binding energies of silver. The result indicated that the synthesized product was composed of silver nanoparticles encapsulated by bioactive compounds present in the mushroom. The reduction of silver nanoparticles was due to the presence of relatively large amount of polyphenols present in the sample. Similar type of study was carried out by using *Aloe vera* and reported that polyphenolic compounds were responsible for the reduction of silver ions[29]. The morphology and nanocrystallite size were determined by the characteristic peak obtained from XRD image. The observed results of FTIR spectra confirmed the presence of aliphatic amines or alcohols representing the presence of polyphenolic compounds. The peaks between 3 250–3 450 cm^{-1} and lesser than 700 cm^{-1} corresponded to the primary aliphatic and aromatic compounds[30], and the peaks round 1 000–1 200 cm^{-1} indicated C-O single band and peak of the carboxyl groups from polyphenolic compounds[31,32].

An attempt has been made to extract the chitosan from chitin isolated from *Fenneropenaeus indicus* (Indian prawn) by various chemical processes and to study the physiochemical properties of prepared chitosan along with commercial chitosan, compared with Korea Food and Drug Administration[33,34]. FTIR analysis represented free amino groups at C2 position of glucosamine, a major band of chitosan[14], therefore confirmed as the chitosan compound. An XRD analysis exposed the typical fingerprints of semi-crystalline chitosan as shown in the results[35]. Yen and Mau found that fungal chitosan showed two crystalline reflections at 9.7° and 19.9°[36]. Kittur *et al*.[37], found that the wide-angle XRD patterns of shrimp chitosan showed two major characteristic peaks at 2θ = 9.9–10.7° and 19.8 -20.7°. It was also reported that the two characteristic crystalline peaks with slightly fluctuated diffraction angles found in the wide angle-X-ray diffraction patterns indicated that two types of α- and γ-chitosan exhibited comparable degree of crystallinity and had two consistent peaks of 9–10° and 19–20°[37].

The transdermal films were prepared with chitosan-gelatin amalgamation with silver nanoparticles. Chitosan is second abundant biopolymer given by nature and has been used in the preparation of the film to give flexibility and rigidity nature. Gelatin is one of hydrolysed compounds of collagen (biopolymer) and animal protein.It gives the elasticity to the film. Glycerol is a moisturizing and plasticizer agent

used in the film preparation. Silver nanoparticles used as binding agent, cross linker and as well as drug provide complete the protection for the film. Then standard values of compounds obtained were then optimized according to the preparation of film. Tensile analyses showed that at a higher concentration of silver nanoparticles, films had higher strength and lower elongation, suggesting that silver salts enhanced cross linking in these films. Glycerol is used as plasticizer for the extension of this film. The reason is that with the increase in plasticizer content, the mobility of chains increases, improving the extensibility and flexibility in the films. The decrease in elongation at 40% plasticizer might be due to the dominating effect of a large proportion of plasticizer decreasing the tensile strength[38].

Physiochemical properties of transdermal film was portrayed by different parameters such as weight and thickness, folding endurance, humidity, absorption and solubility to determine the various characteristics of film towards the wound healing. Uniformity of drug distribution in the film is mandatory to determine the amount of drug released into the wounded site; folding endurance, temperature and pH show the stability of film; humidity and absorption indicate the capacity of film in the absorbing of wound exudate; solubility of film shows the dispersion of drug along with other compound through the wounded site giving the complete protection against the environment and helps in speedy recovery[39-41].

Along with time, the drug released from transdermal film was observed and the release of drug through the dialysis membrane was higher than that in skin permeation study. All data were found to be anomalous diffusion[42]. The transdermal film shows more prominent zone according to the higher concentration of silver nanoparticles. Therefore it shows good zone of inhibition against pathogenic organism, consequently showing the protective role around the wounded area. The MTT assay revealed mild cytotoxicity in the Vero cell line as the concentration of silver nanoparticles increases in the transdermal film. Comparative sort of studies were depicted by using different extracts to compare toxicity[43]. ROS drastically increased during the environmental stress causing damage to living cells. Fluorescent microscope photographs demonstrated the extent of ROS generated. Once the DCF-DA dye diffused into cell line, it is deactelyated into non fluorescent (2',7'-dichlorodihydrofluorescein) but ROS converts into fluorescence compound (2',7'-dichlorofluorescein) [26]. Therefore, in our studies, transdermal films with the higher concentration of silver nanoparticles may prove induction of ROS generation in cells but average concentration shows no signs of ROS generation. Hence, transdermal film is proved as a protective role during inflammation and against ROS generation[44]. Subsequently, it can be taken for further studies.

In conclusion, new transdermal films were prepared with chitosan-gelatin. Biosilver nanoparticles play a binding agent role between both chitosan and gelatin, thus, giving flexibility, stability and prolonged life span for the transdermal film. The film has shown improved water absorption, folding endurance, and also temperature withstanding ability. Silver nanoparticles synthesized from *G. lucidum* gives nanoparticles ranging below 80 nm. The dissolution data indicate the release of the drug determined by the size of nanoparticles. The silver nanoparticles synthesized would be stable in pharmaceutical preparation and it can be easily targeted to specific cells. This gives complete protection to infected site and relives high potentiality against various pathogenic bacteria.

Conflict of interest statement

We declare that we have no conflict of interest.

Acknowledgments

The authors are grateful to the Centre of Nanoscience & Nanotechnology, University of Madras and sophisticated analytical lab of Indian Institute of Technology Madras, Chennai, to carry out the instrumentation works. Also, I appreciate Mr. Joseph Varghese, Mr. Balakumaran and Ms. Tanya Rosebud Fernandes for their valuable support. My special thanks to Dr. Cherian for allowing working in his research institute "Frontier Mediville."

References

[1] National Healing Corporation. Wound healing perspectives: a clinical pathway success advanced therapies. 2005. [Online] Available from: http://www.readbag.com/nationalhealing-downloads-nhcwhpfall05 [Accessed on 15th June, 2015]

[2] Mani H, Sidhu GS, Kumari R, Gaddipati JP, Seth P, Maheshwari RK. Curcumin differentially regulates TGF-beta1, its receptors and nitric oxide synthase during impaired wound healing. *Biofactors* 2002; **16**: 29-43.

[3] Guo S, DiPietro LA. Factors affecting wound healing. *J Dent Res* 2010; **89**(3): 219-29.

[4] Schoellhammer CM, Blankschtein D, Langer R. Skin permeabilization for transdermal drug delivery: recent advances and future prospects. *Expert Opin Drug Deliv* 2014; **11**(3): 393-407.

[5] Gadekar R, Saurabh MK, Thakur GS, Saurabh A. Study of formulation, characterization and wound healing potential of transdermal patches of curcumin. *Asian J Pharm Clin Res* 2012; **5**(Suppl 4): 225-30.

[6] Batra P, Sharma AK, Khajuria R. Probing lingzhi or reishi medicinal mushroom *Ganoderma lucidum* (higher basidiomycetes): a bitter mushroom with amazing health benefits. *Int J Med Mushrooms* 2013; **15**(2): 127-43.

[7] Ko HH, Hung CF, Wang JP, Lin CN. Antiinflammatory triterpenoids and steroids from *Ganoderma lucidum* and *G. tsugae*. *Phytochemistry* 2008; **69**: 234-9.

[8] Li P, Deng YP, Wei XX, Xu JH. Triterpenoids from *Ganoderma lucidum* and their cytotoxic activities. *Nat Prod Res* 2013; **27**(1): 17-22.

[9] Boh B, Berovic M, Zhang J, Zhi-Bin L. *Ganoderma lucidum* and its pharmaceutically active compounds. *Biotechnol Annu Rev* 2007; **13**: 265-301.

[10] Chen Y, Xie MY, Zhang H, Wang YX, Nie SP, Li C. Quantification of total

polysaccharides and triterpenoids in *Ganoderma lucidum* and *Ganoderma atrum* by near infrared spectroscopy and chemometrics. *Food Chem* 2012; **135**: 268-75.

[11] Kumirska J, Czerwicka M, Kaczyński Z, Bychowska A, Brzozowski K, Thöming J, et al. Application of spectroscopic methods for structural analysis of chitin and chitosan. *Mar Drugs* 2010; **8**(5): 1567-636.

[12] Sahoo R, Sahoo S, Nayak PL. Synthesis and characterization of gelatin-chitosan nanocomposite to explore the possible use as drug delivery vehicle. *Eur Sci J* 2013; **9**(18): 135-41.

[13] Lamarque G, Lucas JM, Viton C, Domard A. Physicochemical behavior of homogeneous series of acetylated chitosans in aqueous solution: role of various structural parameters. *Biomacromolecules* 2005; **6**(1): 131-42.

[14] Puvvada YS, Vankayalapati S, Sukhavasi S. Extraction of chitin from chitosan from exoskeleton of shrimp for application in the pharmaceutical industry. *Int Curr Pharm J* 2012; **1**(9): 258-63.

[15] Kumari S, Rath PK. Extraction and characterization of chitin and chitosan from (*Labeo rohit*) fish scales. *Procedia Mater Sci* 2014; **6**: 482-9.

[16] Trunga TS, Thein-Han WW, Qui NT, Ng CH, Stevens WF. Functional characteristics of shrimp chitosan and its membranes as affected by the degree of deacetylation. *Bioresour Technol* 2006; **97**(4): 659-63.

[17] Karwa A, Gaikwad S, Rai MK. Mycosynthesis of silver nanoparticles using Lingzhi or Reishi medicinal mushroom, *Ganoderma lucidum* (W. Curt.:Fr.) P. Karst. and their role as antimicrobials and antibiotic activity enhancers. *Int J Med Mushrooms* 2011; **13**(5): 483-91.

[18] Philip D. Biosynthesis of Au, Ag and Au-Ag nanoparticles using edible mushroom extract. *Spectrochim Acta A Mol Biomol Spectrosc* 2009; **73**: 374-81.

[19] Paul S, Singh ARJ, Sasikumar CS. Green synthesis of bio-silver nanoparticles by *Parmelia perlata*, *Ganoderma lucidum* and *Phellinus igniarius* & their fields of application. *Indian J Res Pharm Biotechnol* 2015; **3**(2): 100-10.

[20] Zhong QP, Xia WS. Physicochemical properties of edible and preservative films from chitosan/cassava starch/gelatin blend plasticized with glycerol. *Food Technol Biotechnol* 2008; **46**(3): 262-9.

[21] Saeed MA. An *in vitro* evaluation of films prepared from gelatin– *Carica papaya* methanolic extract for wound healing. *Int J Drug Deliv* 2013; **5**(2): 233-8.

[22] Soujanya C, Satya BL, Reddy ML, Manogna K, Prakash PR, Ramesh A. Formulation and *in vitro* & *in vivo* evaluation of transdermal patches of lornoxicam using natural permeation enhancers. *Int J Pharm Pharm Sci* 2014; **6**(4): 282-6.

[23] Christian GD, Feldman FJ. *Atomic absorption spectroscopy: applications in agriculture, biology and medicine*. New York: John Wiley & Sons, Inc.; 1970.

[24] Valcarcel M, De Castro MDL. *Flow injection analysis: principles an applications (Ellis Horwood series in analytical chemistry)*. Herts: Ellis Horwood Ltd.; 1987, p. 410.

[25] Manivasagan P, Venkatesan J, Senthilkumar K, Sivakumar K, Kim SK. Biosynthesis, antimicrobial and cytotoxic effect of silver nanoparticles using a novel *Nocardiopsis* sp. MBRC-1. *BioMed Res Int* 2013; doi: 10.1155/2013/287638.

[26] Wu D, Yotnda P. Production and detection of reactive oxygen species (ROS) in cancers. *J Vis Exp* 2011; doi: 10.3791/3357.

[27] Wiley BJ, Im SH, Li ZY, McLellan J, Siekkinen A, Xia Y. Maneuvering the surface plasmon resonance of silver nanostructures through shape-controlled synthesis. *J Phys Chem B* 2006; **110**: 15666-75.

[28] Banerjee J, Narendhirakannan RT. Biosynthesis of silver nanoparticles from *Syzygium cumini* (l.) seed extract and evaluation of their *in vitro* antioxidant activities. *Dig J Nanomater Biostruct* 2011; **6**(3): 961-8.

[29] Song JY, Kim BS. Rapid biological synthesis of silver nanoparticles using plant leaf extracts. *Bioprocess Biosyst Eng* 2009; **32**: 79-84.

[30] Song JY, Jang HK, Kim BS. Biological synthesis of gold nanoparticles using *Magnolia kobus* and *Diopyros kaki* leaf extract. *Process Biochem* 2009; **44**: 1133-8.

[31] Renugadevi TS, Gayathri S. FTIR and FT-Raman spectral analysis of paclitaxel drugs. *Int J Pharm Sci Rev Res* 2010; **2**: 106-10.

[32] Susanto H, Feng Y, Ulbricht M. Fouling behavior during ultrafiltration of aqueous solutions of polyphenolic compounds. *J Food Eng* 2009; **91**: 333-40.

[33] Korea Food and Drug Administration. *Korea food additives code*. Seoul: Korea Food and Drug Administration; 1995, p. 449- 51.

[34] Younes I, Rinaudo M. Chitin and chitosan preparation from marine sources. Structure, properties and applications. *Mar Drugs* 2015; **13**(3): 1133-74.

[35] Bangyekan C, Aht-Ong D, Srikulkit K. Preparation and properties evaluation of chitosan-coated cassava starch films. *Carbohydr Polym* 2006; **63**: 61-71.

[36] Yen MT, Mau JL. Physico-chemical characterization of fungal chitosan from shiitake stipes. *LWT Food Sci Technol* 2007; **40**: 472-9.

[37] Kittur FS, Prashanth KV, Sankar KU, Tharanathan RN. Characterization of chitin, chitosan and their carboxymethyl derivatives by differential scanning calorimetry. *Carbohydr Polym* 2002; **49**: 185-93.

[38] Yen MT, Yang JH, Mau JL. Physicochemical characterization of chitin and chitosan from crab shells. *Carbohydr Polym* 2009; **75**: 15-21.

[39] ASTM International. ASTM D882-12 Standard test method for tensile properties of thin plastic sheeting. West Conshohocken: ASTM International; 2002. [Online] Available from: http://www.astm.org/Standards/D882.htm [Accessed on 20th April, 2015]

[40] Sezer AD, Hatipoğlu F, Cevher E, Oğurtan Z, Baş AL, Akbuğa J. Chitosan film containing fucoidan as a wound dressing for dermal burn healing: preparation and *in vitro/in vivo* evaluation. *AAPS PharmSciTech* 2007; **8**(2): 94-101.

[41] Geil RD, Senkevich JJ, Rogers BR. Method for measuring solvent permeation through polymer film on porous dielectric films. *J Vac Sci Technol* 2009; **27**(4): 1825-28.

[42] Pereira R, Carvalho A, Vaz DC, Gil MH, Mendes A, Bártolo P. Development of novel alginate based hydrogel films for wound healing applications. *Int J Biol Macromol* 2013; **52**: 221-30.

[43] Senthilraja P, Kathiresan K. *In vitro* cytotoxicity MTT assay in Vero, HepG2 and MCF-7 cell lines study of marine yeast. *J App Pharm Sci* 2015; **5**(3): 80-4.

[44] Radek KA, Ranzer MJ, DiPietro LA. Brewing complications: the effect of acute ethanol exposure on wound healing. *J Leukoc Biol* 2009; **86**(5): 1125-34.